

University of Nebraska - Lincoln

DigitalCommons@University of Nebraska - Lincoln

---

Conservation and Survey Division

Natural Resources, School of

---

May 2024

## Theory of an Automatic Seepage Meter and Ramifications for Applications

V. A. Zlotnik

D. K. Solomon

D. P. Genereux

T. E. Gilmore

*University of Nebraska - Lincoln*

C. E. Humphrey

*See next page for additional authors*

Follow this and additional works at: <https://digitalcommons.unl.edu/conservationsurvey>



Part of the [Geology Commons](#), [Geomorphology Commons](#), [Hydrology Commons](#), [Paleontology Commons](#), [Sedimentology Commons](#), [Soil Science Commons](#), and the [Stratigraphy Commons](#)

---

Zlotnik, V. A.; Solomon, D. K.; Genereux, D. P.; Gilmore, T. E.; Humphrey, C. E.; Mittelstet, A. R.; and Zlotnik, A. V., "Theory of an Automatic Seepage Meter and Ramifications for Applications" (2024). *Conservation and Survey Division*. 848.

<https://digitalcommons.unl.edu/conservationsurvey/848>

This Article is brought to you for free and open access by the Natural Resources, School of at DigitalCommons@University of Nebraska - Lincoln. It has been accepted for inclusion in Conservation and Survey Division by an authorized administrator of DigitalCommons@University of Nebraska - Lincoln.

---

**Authors**

V. A. Zlotnik, D. K. Solomon, D. P. Genereux, T. E. Gilmore, C. E. Humphrey, A. R. Mittelstet, and A. V. Zlotnik

# Water Resources Research®



## RESEARCH ARTICLE

10.1029/2023WR034766

## Theory of an Automatic Seepage Meter and Ramifications for Applications

### Key Points:

- A generalized equation of water level dynamics in the Automatic Seepage Meter valid for a variety of field conditions
- The theory considers surface water level fluctuations, evaporation, rainfall, and ambient noise
- Water flux and vertical hydraulic conductivity estimation accuracy is analyzed with examples and recommendations

### Supporting Information:

Supporting Information may be found in the online version of this article.

### Correspondence to:

V. A. Zlotnik,  
vzlotnik1@unl.edu

### Citation:

Zlotnik, V. A., Solomon, D. K., Genereux, D. P., Gilmore, T. E., Humphrey, C. E., Mittelstet, A. R., & Zlotnik, A. V. (2023). Theory of an automatic seepage meter and ramifications for applications. *Water Resources Research*, 59, e2023WR034766. <https://doi.org/10.1029/2023WR034766>






Received 2 MAR 2023  
Accepted 15 SEP 2023

### Author Contributions:

**Conceptualization:** Vitaly A. Zlotnik, D. Kip Solomon, Anatoly V. Zlotnik  
**Data curation:** D. Kip Solomon  
**Formal analysis:** Vitaly A. Zlotnik, D. Kip Solomon, Anatoly V. Zlotnik  
**Investigation:** Vitaly A. Zlotnik, D. Kip Solomon, Troy E. Gilmore, C. Eric Humphrey, Aaron R. Mittelstet  
**Methodology:** Vitaly A. Zlotnik, D. Kip Solomon, Anatoly V. Zlotnik  
**Resources:** Troy E. Gilmore, Aaron R. Mittelstet

© 2023. The Authors.

This is an open access article under the terms of the [Creative Commons Attribution-NonCommercial-NoDerivs License](#), which permits use and distribution in any medium, provided the original work is properly cited, the use is non-commercial and no modifications or adaptations are made.

Vitaly A. Zlotnik<sup>1</sup> , D. Kip Solomon<sup>2</sup> , David P. Genereux<sup>3</sup> , Troy E. Gilmore<sup>4</sup> ,  
C. Eric Humphrey<sup>2</sup> , Aaron R. Mittelstet<sup>5</sup>, and Anatoly V. Zlotnik<sup>6</sup>

<sup>1</sup>Department of Earth and Atmospheric Sciences, University of Nebraska-Lincoln, Lincoln, NE, USA, <sup>2</sup>Department of Geology and Geophysics, University of Utah, Salt Lake City, UT, USA, <sup>3</sup>Department of Marine, Earth, and Atmospheric Sciences, North Carolina State University, Raleigh, NC, USA, <sup>4</sup>School of Natural Resources, University of Nebraska-Lincoln, Lincoln, NE, USA, <sup>5</sup>Biological Systems Engineering Department, University of Nebraska-Lincoln, Lincoln, NE, USA, <sup>6</sup>Applied Mathematics and Plasma Physics (T-5), Los Alamos National Laboratory, Los Alamos, NM, USA

**Abstract** A new approach for measuring fluxes across surface water—groundwater interfaces was recently proposed. The Automatic Seepage Meter (ASM) is equipped with a precise water level sensor and digital memory that analyzes water level time series in a vertical tube inserted into a streambed (Solomon et al., 2020, <https://doi.org/10.1029/2019WR026983>). The ability to infer flux values with high temporal resolution relies on an accurate interpretation of water level dynamics inside the tube. Here, we reduce the three-dimensional hydrodynamic problem that describes the ASM water level in a variety of field conditions to a single ordinary differential equation. This novel general analytical solution for estimating ASM responses is more comprehensive and flexible than previous approaches and is applicable to the entire range of field conditions, including steady or transient stream stages, evaporation, rainfall, and noise. For example, our analysis determines the timing of the nonmonotonic ASM response to a monotonic linear stream stage variation and explains previously used empirical parabolic approximation for estimating fluxes. We present algorithms for simultaneous inference of vertical interface flux and hydraulic conductivity values together with an example code. We quantify how the accuracy of parameter estimation depends on test duration and noise amplitude and propose how our analysis can be used to optimize field test protocols. On this basis, changing the ASM geometry by increasing the radius and decreasing tube insertion depth may enable ASM field test protocols that estimate interface flux and hydraulic conductivity faster while maintaining desired accuracy. Potential applications of joint parameter estimation are suggested.

## 1. Introduction

Determining groundwater fluxes in streams, lakes, estuaries, and submarine areas is a challenging problem in the field of surface water-groundwater interactions. In this context, the term *stream* is used for any surface water synonymously, and the term *interface* is defined as the near-horizontal surface separating surface water from the subsurface sediments. Summaries of various methods to estimate water flux through streambeds indicate potentially lengthy sampling times (at the scale of a day or more), which result in averaging of varying fluxes over long periods (e.g., Cremeans et al., 2020; Gilmore et al., 2016; Rosenberry & Hayashi, 2013; Rosenberry et al., 2008; Zlotnik & Tartakovsky, 2018; Zlotnik et al., 2016). Previously published point-scale methods require less time, usually a half-hour or less per point, but are not suited to continuous remote monitoring of streambed water flux (Gilmore et al., 2016; Kennedy et al., 2009, 2010).

To address the challenge of rapidly estimating time-varying flux rates, collecting and storing data in a digital format under designed test programs, and other technical issues (Solomon et al., 2020), presented a new Automatic Seepage Meter (ASM) and the results of associated field studies. The ASM test is based on the open-bottom permeameter (OBP), a.k.a. tube method, which was studied and summarized by Bouwer (1978, Section 5.3.3). This tube method is commonly used in studies of streambed properties and other applications (Chen et al., 2009; Kennedy et al., 2009, 2010; Landon et al., 2001; Pétré et al., 2021).

In this study, we present a theory to synthesize and advance previously scattered methodological foundations of the ASM test. We focus on theoretical and numerical aspects in light of differences between the ASM and the slug test, without additional modifications of instrumentation or field aspects. We suppose that vertical fluxes

**Software:** Vitaly A. Zlotnik, Anatoly V. Zlotnik

**Validation:** Vitaly A. Zlotnik

**Visualization:** Vitaly A. Zlotnik

**Writing – original draft:** Vitaly A. Zlotnik

**Writing – review & editing:** Vitaly A. Zlotnik, D. Kip Solomon, David P. Genereux, C. Eric Humphrey

across the streambed, hydraulic conductivity, measurement noise, and estimation accuracy can be characterized simultaneously at each tested position for interpretation in the field.

Our presentation proceeds as follows: In Section 2, we introduce a three-dimensional (3D) hydrodynamic ASM model that is reduced accurately to a single ordinary differential equation that is valid for a variety of initial conditions and operating forces, including seepage fluxes, evaporation, precipitation, variable stream stage, and noise in the collected data. In Section 3, we apply the derived equation for stream stage conditions with steady-state and varying water levels. We derive compact and convenient analytical solutions to account for the integrated influence of all factors, namely, streambed properties, the shape factor of the tube, the rates of evaporation and precipitation for the upper chamber during a test, and variable stream stage. A linear model of the stream stage can be used to give a general explanation of some cases of nonmonotonic behavior of the water level in the ASM. Moreover, the meaning of parameters of the empirical parabolic curve that was previously used to interpret data is clarified.

In Section 4, we present statistical analyses that explore the role of noise in the field data. The noise is attributed to both environmental sources and instrumentation factors for different hydrological conditions. Using a steady-state approximation model for the stream stage, the accuracy of joint identification of seepage flux and hydraulic conductivity is investigated, and optimal test duration values are given. We show that a previous approach may be modified to reduce test duration. In Section 5, we examine the implications of the estimation method for interpreting typical field data, modifying instrumentation design, field protocols, and analyzing test results that were previously published for ASM applications, and summarize our conclusions in Section 6.

## 2. Hydrodynamic ASM Model

The purpose of the hydrodynamic model in this study is to derive an equation for the water level in the upper chamber of the ASM based on the hydrodynamics of the flow near and inside the ASM, the rate of evaporation and precipitation, and measurement noise characteristics.

An ASM measurement begins with vertical insertion of a thin-walled hollow tube of radius  $R$  across the surface water-groundwater interface to a depth  $L$ , as illustrated in Figure 1. This leaves the ASM with a sediment-filled “lower chamber” and water-filled “upper chamber.” The depth  $L$  is typically substantially larger than the radius  $R$  to assure stability of the tube in the streambed and evaluate the seepage flux below the hyporheic zone. The tube is fitted with a valve in the tube wall that opens or closes the connection between the tube and the stream water when activated by a programmed microcontroller. Operation of the valve produces a time-variable water flux across the sediment-water interface inside the tube. The head space above the water level in the tube is fitted with a highly precise ( $\pm 0.1$  mm) device that is set to monitor the transient water level. The design and technical details of this instrument were presented by Solomon et al. (2020), and in this study, we focus on the principles of its operation that play a role in hydrodynamic analyses for estimating vertical interface flux and vertical hydraulic conductivity.

In natural conditions, the flux at the horizontal surface water-groundwater interface is normal to the interface and is assumed near-vertical due to the near-horizontal interface with constant head and is directed downward or upward in the case of a losing or gaining stream, respectively. Alterations of head gradients in response to small features, such as streambed ripples, are usually local, decrease exponentially with depth, and can be ignored relative to the insertion depth of the permeameter (Bardini et al., 2013; Boano et al., 2014). The water level both outside and inside the tube is  $H_S$  when the valve is open. Closing the valve perturbs the natural subsurface flux field locally and dynamically in time (Figure 1b), but the magnitude of perturbation of the water level in the tube and local flux distribution in its vicinity are negligible at the initial moment. The rising water level inside the tube increases hydrostatic pressure at the water-sediment interface inside the ASM, through the open bottom. As a result, the upward flux into the tube through the open bottom eventually ceases when the hydrostatic pressure on the interface reaches  $H_S + H_{\max}$ , which is the terminal water level inside of the permeameter. Values of  $H_{\max}$  can be positive or negative, and therefore, the earliest water level dynamics can be used for inference of the initial natural water flux through the streambed. This is because the streambed flow net is in steady state at the start of the test, i.e., the moment when the valve first closes (e.g., Chen et al., 2009; Solder et al., 2016; Solomon et al., 2020). The rapidly changing head gradient during the first few seconds following valve closure is directly related to both the initial vertical seepage rate and the reduction in vertical flow through the permeameter.

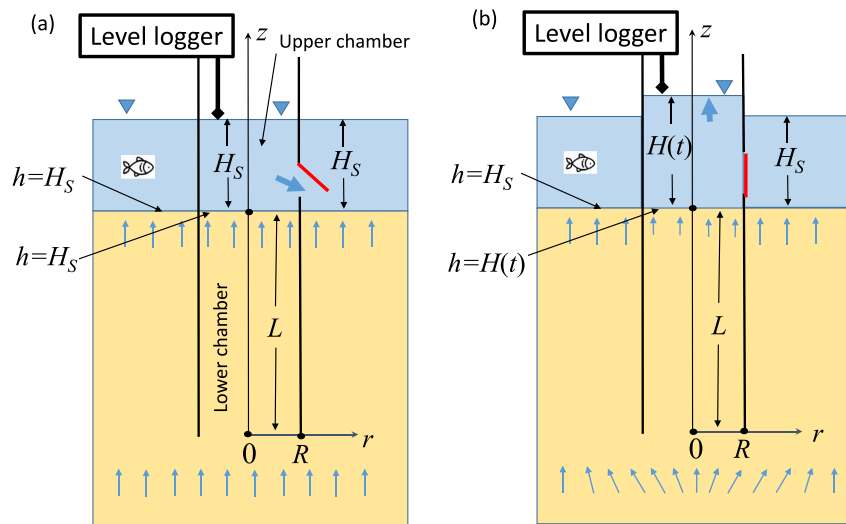


**Figure 1.** Automatic Seepage Meter operation in a gaining stream: (a) pretest conditions when the valve (in red) is opened; the water level is equal to the stream level due to this connection, and streamlines are vertical in the subsurface (blue arrows show local directions); and (b) test initiation by valve closure. Immediately after closure, the local flux directions are rearranged as shown schematically below the tube bottom, and the upward groundwater flux results in a water level rise in the upper chamber. Here,  $r$  and  $z$  are radial and vertical coordinates, respectively.

Ambient stream turbulence, stream stage variations, and instrumentation errors all add noise to the water level dynamics both outside and inside the tube. The rise (or fall) of the water level in the upper chamber with respect to the initial stream stage is on the order of few mm or cm in most cases. This stabilization was accomplished using a differential pressure transducer (Solder et al., 2016) initially, which was subsequently replaced by an electromechanical ASM (Solomon et al., 2020). These studies focused on hardware, simplified data interpretation for the steady-state stream stage using a basic model, ad hoc analyses of accuracy, and examples of possible ASM responses to time-variable stream stage. Numerous measurements using this instrument were made by Humphrey et al. (2022).

In earlier studies, only the initial segment of the water level time series was used for calculating the flux by fitting parabola to the initial segment. Subsequently, slug test interpretations that did not consider the specifics of an open bottom were made separately for inference of hydraulic conductivity when needed. However, the accuracy of each of these two characteristics depends on the entire curve, i.e., both parameters should be determined simultaneously, with estimates of accuracy. The accuracy and efficiency of flux parameter estimation using water level data can be improved if a general equation for water level dynamics in the ASM is derived rigorously based on the hydrodynamics in sediments inside and outside the ASM tube together with the characteristics of noise in the water level data.

## 2.1. ASM Problem Statement

The total hydraulic head  $h(r, z, t)$  in the streambed is considered a function of time  $t$  and location in cylindrical coordinates, where  $r$  is the radial coordinate and  $z$  is a vertical coordinate with positive orientation upward (Figure 1). The anisotropic uniform streambed has uniform horizontal hydraulic conductivity  $K_r$ , vertical hydraulic conductivity  $K_z$ , and specific storage  $S_s$ . In undisturbed conditions, the head in the subsurface beneath the interface is denoted as  $h_0(r, z, t)$  and is a linear function of depth in the vicinity of the tube, given by

$$h_0(r, z, t) = H_S(t) - \frac{q_z}{K_z}(z - L), \quad h_0(r, L, t) = H_S(t), \quad -\infty < z < L \quad (1)$$

where  $q_z$  is the vertical water flux in the sediments. Here,  $L$  is the elevation of the horizontal water-sediment interface above the tube bottom, and the general transient water level in the stream,  $H_S(t)$ , may change on the hourly scale. Fluxes across the interface are determined by hydraulic head gradient  $(-q_z/K_z)$ , and may vary on the same, or much longer, time scale. The head at the interface is equal to the surface water elevation.

After the test is initiated by closure of the valve, the head dynamics in the sediments inside and outside the tube of radius  $R$  are described by the equation for subsurface flow, given by

$$S_s \frac{\partial h}{\partial t} = \frac{K_r}{r} \frac{\partial}{\partial r} \left( r \frac{\partial h}{\partial r} \right) + K_z \frac{\partial^2 h}{\partial z^2}, \quad 0 < r < \infty, -\infty < z < L, t > 0 \quad (2)$$

with initial condition

$$h(r, z, 0) = h_0(r, z, 0), \quad 0 < r < \infty, -\infty < z < L \quad (3)$$

and boundary conditions

$$\frac{\partial h(r, z, t)}{\partial z} = -\frac{q_z}{K_z}; \quad r \geq 0, z \rightarrow -\infty; \quad r \rightarrow \infty, \quad -\infty < z < L \quad (4)$$

$$\frac{\partial h(0, z, t)}{\partial r} = 0, \quad -\infty < z < L \quad (5)$$

$$\frac{\partial h(R, z, t)}{\partial r} = 0, \quad 0 < z < L \quad (6)$$

$$h(r, L, t) = \begin{cases} H(t), & r < R \\ H_S(t), & r > R \end{cases} \quad (7)$$

To formulate Equation 4, we assume that the natural flow conditions are undisturbed at large depths and radial distances from the ASM at scales on the order of  $R$  radially and  $L$  vertically. We also assume a uniform initial velocity profile if the stream stage has been steady for some time before the test. In practice, this assumption is difficult to ascertain because of interplay between the stream stage and variable interface fluxes. Equation 5 indicates the axial symmetry of the problem. Equation 6 describes the tube walls as an impermeable lateral boundary. Finally, Equation 7 indicates that the head distribution  $h(r, z, t)$  at the interface inside and outside the upper chamber may differ at various moments, i.e.,  $H(t) \neq H_S(t)$ . This difference between the head values leads to the exchange of water between the upper chamber and the lower chamber through the interface in a dipole-type fashion (e.g., Tartakovsky et al., 2000; Zlotnik & Ledder, 1996). This explains the reason of localization of the flow within the domain at a scale on the order of  $R$  radially and  $L$  vertically.

An additional equation that is needed for determining the unknown function  $H(t)$  is obtained from the water balance. It includes the discharge  $Q(t)$  into the upper chamber across the interface, given by

$$Q(t) = -2\pi K_z \int_0^R \frac{\partial h(r, L, t)}{\partial z} r dr \quad (8)$$

as well as the difference  $E(t)$  between the rates of evaporation from and precipitation into the upper chamber:

$$\pi R^2 \frac{dH}{dt} = -2\pi K_z \int_0^R \frac{\partial h(r, L, t)}{\partial z} r dr - E\pi R^2, \quad H(0) = H_0 \quad (9)$$

The quantity  $E(t)$  is often inconsequential for a single measurement, but estimates must be available for specific weather conditions and variations. The initial condition of the water level in the upper chamber defines the test setup. The dynamics of the water level are driven by the interplay of the natural vertical seepage flux through the bottom of the upper chamber with evaporation and precipitation. The solutions for  $h(r, z, t)$  and  $H(t)$  are defined uniquely by coupling Equations 2 and 9 with the corresponding boundary and initial conditions in Equations 3–7. The variable  $H(t)$  is observable by a measurement that is used for inference of the transient flux  $q_z$ , and this is the focus of our study.

## 2.2. Transformation of the ASM to the Open Bottom Permeameter Problem

The ASM test utilizes a configuration of the OBP for slug tests, but with a different test initiation. Slug tests are triggered by a rapid removal or addition of a controlled water volume (slug), which results in a head difference between the upper chamber and the stream, which then dissipates through the lower chamber. In contrast, the ASM operates by changing the interface between the upper chamber and the stream, and thus does not require a slug. The hydrodynamic 3D treatment of OBP problems was given by Zlotnik et al. (2021). In such problems, the compressibility  $S_s$  is safely neglected in the subsurface flow Equation 2.

The boundary value problem (BVP) for the drawup  $s(r, z, t)$ , which is defined as an increase of the head distribution over its initial state by

$$s(r, z, t) = h(r, z, t) - h_0(r, z, 0) \quad (10)$$

is obtained from the following system of equations:

$$\frac{K_r}{r} \frac{\partial}{\partial r} \left( r \frac{\partial s}{\partial r} \right) + K_z \frac{\partial^2 s}{\partial z^2} = 0, \quad 0 < r < \infty, -\infty < z < L_E \quad (11)$$

$$s(r, z, 0) = 0, \quad 0 < r < \infty, -\infty < z < L \quad (12)$$

$$\frac{\partial s(r, z, t)}{\partial z} = 0; \quad r \geq 0, z \rightarrow -\infty; \quad r \rightarrow \infty, -\infty < z < L \quad (13)$$

$$\frac{\partial s(0, z, t)}{\partial r} = 0, -\infty < z < L \quad (14)$$

$$\frac{\partial s(R, z, t)}{\partial r} = 0, 0 < z < L \quad (15)$$

$$s(r, L, t) = \begin{cases} H(t) - H_S(t), & r < R \\ 0, & r > R \end{cases} \quad (16)$$

The BVP defined by Equations 11–16 has been studied extensively since Hvorslev (1951, p. 44, Figure 18, Case E). It is of special interest to characterize the discharge  $Q_{\text{OBP}}(t)$  across the interface between the lower and upper chambers, which is given by

$$Q_{\text{OBP}}(t) = -2\pi K_z \int_0^R \frac{\partial s(r, L, t)}{\partial z} r \, dr \quad (17)$$

The linearity of the BVP by Equations 11–16 yields a linear relationship between  $Q_{\text{OBP}}(t)$  and head difference  $H(t) - H_S(t)$ , which takes the form

$$\frac{Q_{\text{OBP}}(t)}{\pi R^2} = -K_z \frac{H(t) - H_S(t)}{L \cdot F}, \quad t > 0 \quad (18)$$

in which a negative sign indicates downward flux if  $H(t) > H_S(t)$ , and where  $F$  is a dimensionless constant called the *shape factor*. This equation reduces essentially to Darcy's equation for the lower chamber in the case that  $F = 1$ . The shape factor  $F$  depends on the test geometry and aquifer hydraulic properties (Zlotnik et al., 2021). When the tube radius  $R$  is much smaller than the tube length  $L$ , the following approximation can be used (Bouwer, 1978; Chen et al., 2009; Landon et al., 2001, p. 874, Figure 2, Equation 4)

$$F = 1 + \frac{\pi R}{5.5 L} \sqrt{\frac{K_z}{K_r}} \quad (19)$$

The above result was extensively reanalyzed and applied in practice (Pozdnyakov et al., 2016, Equation 22 and p. 140) verified this result rigorously using finite differences and showed that Equation 18 has an accuracy on the order of 1% for  $R/L < 1/6$ , which is consistent with Bouwer (1978, Table 5.68). With respect to the anisotropy



effect of hydraulic conductivity on the values of  $F$ , Burger and Belitz (1997) indicated that the ratio  $K_r/K_z$  ranges between 1 and 10 for unconsolidated sand and gravel fluvial sediments in samples of size comparable with the lower chamber length of the ASM, and this can be used to calibrate the accuracy of Equation 19 in general. Zlotnik et al. (2021) provided detailed analyses of  $F$  for a wide range of values of the parameters  $R/L$  and  $K_r/K_z$ . Based on Equations 1, 8, and 17, the relationship between  $Q_{\text{OBP}}(t)$  and  $Q(t)$  takes the form

$$Q(t) = \pi R^2 q_z + Q_{\text{OBP}}(t) \quad (20)$$

The term  $\pi R^2 q_z$  in Equation 20 above describes the undisturbed natural volumetric flux into the upper chamber, which is positive in gaining streams, as shown in Figure 1a. A simultaneous opposite discharge  $Q_{\text{OBP}}(t)$ , which is negative or downward in gaining streams, is driven by the difference between the water level in the upper chamber of the ASM and the stream level when  $H(t) \neq H_s(t)$ .

### 2.3. Hydraulic Role of the Lower ASM Chamber in Stream-Aquifer Exchange

The mechanism of water exchange between the upper chamber and the stream occurs through the streambed sediments inside the lower chamber and streambed sediments outside the tube. Solder et al. (2016) and Solomon et al. (2020) used a small  $R/L$  ratio to ensure mechanical stability of the ASM setup by deep penetration into the streambed, to minimize noise in the ASM readings, and enable use of a simplified estimate with shape factor  $F = 1$ . In that case, Equation 19 yields  $F \approx 1$  in isotropic streambeds and becomes more accurate for streambeds with higher anisotropy ratio.

This finding is critical for understanding and differentiating the role of the streambed sediments inside and outside the lower chamber in the 3D flow system. As we indicate above, in the case that  $F = 1$  then Equation 18 is exactly Darcy's law for specific discharge  $Q_{\text{OBP}}(t)$  through the sample of length  $L$ , and this results because of the head difference  $H(t)$  between the top of the lower chamber and the bottom of the lower chamber, where the stream stage head is denoted  $H_s(t)$ . However, the head at this bottom point of the ASM deviates from  $H_s(t)$ , because  $F$  exceeds 1 by  $<0.09$  when  $R/L < 1/6$  and conditions are isotropic (see Zlotnik et al., 2021). Such parameter values indicate minor hydraulic resistance at the interface between sediments at the bottom of the tube and the streambed immediately external to the tube. Thus, the resistance of sediments inside the lower ASM chamber (of length  $L$ ) is  $>11$  times higher for the existing ASM design, and the external resistance of the sediments outside the tube can be neglected. In the absence of clearly defined vertical contrasts, the layered heterogeneity of the sediments at this scale in slug tests can typically be neglected (e.g., Burnette et al., 2016). Values of  $F \approx 1$  indicate that additional “external resistance is not essential because the main hydraulic resistance is concentrated inside the pipe” (Pozdnyakov et al., 2016, p. 140). Therefore, flow within the lower ASM chamber is the major process to be accounted for in theoretical and practical analysis for such geometry (e.g., Chen, 2000; Chen et al., 2009; Liu et al., 2018). This result quantitatively explains the “shifting” of the head value from the streambed surface to the bottom of the lower ASM chamber at the depth  $L$ , even after transition of the stream stage. Other configurations with more desirable characteristics can be explored, e.g., a larger radius and shallow penetration. In such designs, large values  $F \gg 1$  of the shape factor are possible (Zlotnik et al., 2021).

## 3. Operational ASM Test Model

### 3.1. General Solution

Equations 18 and 20 are critical to a transformation of the BVP 2–7 and 9 to enable derivation of an operational model for the dynamics of the water level  $H(t)$  as measured by the ASM. Their substitution into Equation 9 yields an ordinary linear differential equation (ODE)

$$\frac{dH}{dt} = -\frac{H - H_s}{t_L} + q_z - E, \quad H(0) = H_0, t_L = \frac{L \cdot F}{K_z} \quad (21)$$

The parameter  $t_L$  in Equation 21 is commonly called the time lag, and was introduced by Hvorslev (1951). For the ASM geometry of (Solomon et al., 2020), one can assume that  $F \approx 1$  when defining  $t_L$ . Otherwise, the method for determining  $F$  in Zlotnik et al. (2021) can be applied. In addition, estimates of  $E$  should be available for interpretation of ASM test data, and Equation 21 admits a time-dependent  $E$ . This rate  $E$  may be on the order of several mm a day, which can be significant in situations where the magnitude of the flux  $q_z$  is small.



Solomon et al. (2020) proposed that the instantaneous flux can be obtained using the initial part of the water level measurement time series directly using Equation 20. Opening of the valve prior to the test guarantees equivalent initial levels inside and outside the ASM, i.e.,  $H(0) = H_S(0)$ , in which case the form of Equation 21 at the moment of valve closure is

$$q_z = \frac{dH(0)}{dt} + E, \quad t = 0 \quad (22)$$

The form of Equation 22 gives the slope ( $dH(0)/dt$ ) of the parabolic change in water level recorded in the upper ASM chamber at the initial moment. It is assumed that this approach yields the constant seepage flux over time on the order of the time lag  $t_L$ , when corrected by the rates of evaporation and precipitation. As in the general case of Equation 21, the value of  $E$  may be important with small flux  $q_z$ . In discretized form, Equation 21 can be used for deriving the time-dependent seepage rate  $q_z(t)$  if  $H_S(t)$  can be obtained independently by another ASM with an open valve or a pressure transducer. The general solution for the water level in the upper ASM chamber that accounts for stream stage variations  $H_S(t)$ , together with effects of  $q_z$  and  $E$  during the ASM test can be presented (as shown in Text S1 in Supporting Information S1) as follows:

$$H(t) = H(0)e^{-t/t_L} + \frac{1}{t_L} e^{-t/t_L} \int_0^t [H_S(t') + t_L(q_z - E)] e^{t'/t_L} dt' \quad (23)$$

### 3.2. Basic Solution: Case of Steady-State Stream Stage

We suppose that prior to the test, water levels in the stream and inside the ASM are identical, i.e.,  $H_S(t) = H_0$ . We also consider a flux that does not change over the test duration, i.e.,  $q_z \equiv \text{const.}$  and  $E = 0$ . These assumptions are valid if the test time is short compared to diurnal variations, or if the variations are small.

#### 3.2.1. Closed Form Solution

After substitution into Equation 23, integration results in an equation for water level dynamics in the upper chamber of the form

$$H(t) = H_0 + H_{\max}(1 - e^{-t/t_L}), \quad H_{\max} = q_z t_L \quad (24)$$

where  $H_{\max}$  is the terminal water level change in the upper chamber with respect to an initial stream stage that has been steady for a long run, i.e.,  $t \gg t_L$ . For losing streams, we suppose that  $q_z$  and  $H_{\max}$  are negative. Solomon et al. (2020) used this equation by making a partial analogy with slug tests, but the hydrogeological meaning of  $H_{\max}$  was not investigated in that study.

We emphasize the importance of the physical parameter  $H_{\max}$ , which explicitly incorporates the dependence on streambed properties  $K_r$  and  $K_z$ , the local flux  $q_z$ , and the test geometry  $R$  and  $L$ . In fact, the ASM acts as a piezometer, but with an open finite-radius bottom (Zlotnik et al., 2021). Therefore, the values of  $H_{\max}$  likely will vary depending on the penetration depth and radius. To account for evaporation and precipitation, the value of  $q_z$  should be replaced with  $q_z - E$ , where  $E$  must be estimated or known over the test time, but this was not the approach applied previously (Solomon et al., 2020).

#### 3.2.2. Parabolic Approximation of Solution

In previous studies, the early part of the time series was approximated by a general parabola (Solder et al., 2016) and used to estimate  $q_z$ . It is informative to consider the physical meaning of the coefficients of a parabolic estimate. For short times, the three-term Taylor expansion of the exponent in Equation 24 is given by

$$H(t) \approx H_0 + q_z t - 0.5 \cdot q_z t^2 / t_L = H_0 + q_z \cdot t(1 - 0.5t/t_L) \quad (25)$$

The parabola in Equation 25 depends on the parameters  $q_z$  and  $t_L$ , and provides an accuracy better than 2% when  $t < 0.4 \cdot t_L$ . However, the quadratic term in Equation 25 includes the time lag  $t_L$  explicitly, and more information can be extracted from this coefficient by fitting Equation 25 to a time series of measurements of  $H(t)$ . For even shorter times ( $t < 0.1 \cdot t_L$ ), the two-term expansion

$$H(t) \approx H_0 + q_z t \quad (26)$$

yields a straight line with accuracy better than 0.5%. Thus,  $q_z$  can be estimated by regression analysis if a time series of observations of  $H(t)$  is available for the early test period. If  $K_z$  can be independently found or estimated, one can infer the time lag  $t_L$  (see Section 4.1).

### 3.3. ASM Responses to Varying Transient Stream Stage

There are a variety of ways to characterize the variations of  $H(t)$  under different stream stage functions  $H_S(t)$ , of which linear, piecewise linear, and piecewise constant are the most representative.

#### 3.3.1. Linear Stream Stage

Sometimes, the stream stage  $H_S(t)$  can be approximated by a linear function between start time  $t = 0$  and end time  $t_{\text{end}} = t_1$  as follows:

$$H_S(t) = H_0 + p \cdot t, \quad p = [H_S(t_{\text{end}}) - H_0]/t_1, \quad 0 < t < t_{\text{end}} = t_1 \quad (27)$$

where  $H_S(t_{\text{end}})$  is the stream stage at the test end time  $t_{\text{end}}$ . In the case that  $q_z \equiv \text{const.}$  and  $E = 0$ , the substitution of  $H_S(t)$  into Equation 23 and integration (see Text S1 in Supporting Information S1) result in an ASM response of the form

$$H(t) = H_S(t) + t_L(q_z - p)(1 - e^{-t/t_L}) \quad (28)$$

Counterintuitively, a monotonic linear change of the stream stage may result in a nonmonotonic response of the ASM water level, when the vertical flow in the upper chamber of the ASM changes direction at some moment  $t_{\text{ch}}$  (Solomon et al., 2020, an example in Supporting Information there). The timing  $t_{\text{ch}}$  of reversal in the flow direction  $t_{\text{ch}}$  can be found in terms of the parameters of the ASM and the aquifer. It occurs at the time when the derivative of  $H(t)$  is equal to zero, i.e.

$$t_{\text{ch}} = t_L \ln(1 - q_z/p), \quad 0 < 1 - q_z/p < \infty \quad (29)$$

#### 3.3.2. Piecewise-Linear Stream Stage

A compact analytical solution for the stream stage  $H_S(t)$  can be derived when the hydrograph is approximated by  $I$  linear segments. Because the ASM measures the water level in the upper chamber, which is separated from the stream by a closed valve after initiating the test (see procedures in Section 1, Figure 1), another instrument is needed for acquisition of  $H_S(t)$ . This can be another ASM or a pressure transducer of adequate accuracy. Each of the  $I$  segments may have a different duration and include different numbers of intermediate data points. By interpolating the stream stage measurements  $H_{S,i}(t) = H_S(t_i)$  between sample times  $t_i$ , where  $i = 0, 1, \dots, I$  and  $H_{S,0}(0) = H(0) = H_0$  at test initiation time ( $t = 0$ ), the hydrograph is obtained as

$$H_S(t) = H_{S,i} + p_i(t - t_i), \quad t_i < t < t_{i+1} \quad (30)$$

with segment slopes  $p_i$

$$p_i = \frac{H_{S,i+1} - H_{S,i}}{t_{i+1} - t_i}, \quad i = 0, 1, 2, \dots, I - 1 \quad (31)$$

The analytical solution at time  $t_1$  is obtained by substitution of the hydrograph into Equation 23 and integration, which results in

$$H(t_1) = H(0)e^{-s_I} + H_{\text{max}}(1 - e^{-s_I}) + \sum_{i=0}^{I-1} \left\{ e^{-(s_I - s_i)} (H_{S,i} - p_i t_L) (e^{\delta_i} - 1) + p_i t_L e^{-(s_I - s_{i+1})} \delta_i \right\} \quad (32)$$

where

$$s_I = t_1/t_L, \quad s_i = t_i/t_L, \quad \delta_i = s_{i+1} - s_i \quad (33)$$

### 3.3.3. Stepwise Change of Stream Stage Record With Uniform Time Intervals

Consider stream stage  $H_S(t)$  that starts at zero at the initial time, and equals the level in the ASM, i.e.,  $H(0) = H_{S,0} = 0$ . In general, the stream stage changes in irregular fashion and the data must be collected frequently at equal intervals  $\Delta t$ , resulting in sample times  $t_i = i\Delta t$  for  $i = 0, 1, \dots, J$ . After integration, the ASM response  $H(t_i)$  at the terminal time  $t_i = I\Delta t$  can be written as

$$H(t_I) = H_{\max} \left( 1 - e^{-\frac{t_I}{t_L}} \right) + H_{S,I} - \sum_{i=0}^{I-1} \Delta H_{S,i} e^{-\frac{(I-i)\Delta t}{t_L}}, \quad \Delta H_{S,i} = H_{S,i+1} - H_{S,i} \quad (34)$$

Equation 34 can be used for irregular stream stage variations  $H_S(t_i)$ , but the accuracy of the results depends on  $\Delta t$ . It can be shown that Equation 34 converges to Equation 28 for linear stream stage as given by Equation 27 if increments  $\Delta H_{S,i} \equiv H_S(t_{i+1}) - H_S(t_i)$  of the stream stage are identical between sampling time intervals, i.e.,  $\Delta H_S \equiv \Delta H_{S,i} \equiv p \cdot \Delta t$  for some constant value of  $p$ .

## 4. Effect of Noise on ASM Applications for Flux and Hydraulic Conductivity Analyses

### 4.1. Test Characteristics in Different Environments

Field data collections of water level series are usually subject to noise, which reflects both short-term stream-stage variability and measurement errors, and as a result any inference of  $q_z$  and  $K_z$  from such data have some error as well. The three parameters that define the ASM setup are (a) penetration depth of the tube into the streambed ( $L$ ); (b) the error in water level measurement instrumentation together with the ambient noise; and (c) test duration. The penetration must be deep enough to provide vertical tube stability. Previous studies have used a permeameter tube of 0.07 m radius and a preferred depth of 0.3 m (Solder et al., 2016; Solomon et al., 2020). To investigate the role of ambient noise and test duration, ranges of parameters must be assessed.

We observe empirically that adequate estimation can be accomplished with brief measurement duration in the case that  $q_z$  is the only parameter of interest. The need for longer measurement duration may become a concern when both  $q_z$  and  $K_z$  must be determined in a fine-grained sediment, although tests may yield insufficient measurements even in massive ASM campaigns in coarse-grain sediments. The expected range of the terminal water level rise  $H_{\max}$  is determined by the magnitude of  $q_z$  and the time lag  $t_L$ , which depend on  $L$  and  $K_z$ . The magnitude of  $q_z$  is typically observed to range between 0 and 1 m day<sup>-1</sup>, and takes higher values in streams than in the lakes (Cremeans et al., 2020; Glose et al., 2019). The time-lag value can be estimated as  $t_L \approx L/K_z$  with an assumption of  $F \approx 1$  used in Equation 21. A study by Calver (2001) reported ranges of streambed  $K_z$  values between  $1.0 \times 10^{-7}$  m s<sup>-1</sup> (0.01 m day<sup>-1</sup>) and  $1.0 \times 10^{-3}$  m s<sup>-1</sup> (100 m day<sup>-1</sup>), and this is a typical range for most field conditions. Thus,  $t_L$  ranges from 300 s (about 1/300 days, or 5 min) to  $0.3 \times 10^7$  s (about 30 days), and the value of  $H_{\max}$  can thus theoretically be as low as 0.0035 m, which creates issues related to selecting an appropriate method of water level measurement. In particular, to be useful for small values of  $H_{\max}$ , the accuracy of the level measurements must be on the order of  $10^{-4}$  m, which is indeed achieved by the ASM presented by Solomon et al. (2020).

Based on the general analyses described in Section 3.3, the parameter  $q_z$  can be obtained using short-duration tests. However, accurate inference of  $K_z$  in the same location can be realized only when the test end time  $t_{\text{end}}$  is on the order of  $t_L$ , and the curvature of the water level time series graph becomes apparent (Solomon et al., 2020). Therefore, the specification of the range of  $K_z$  for the site is recommended by using a typical range of parameters according to the sediment type present (e.g., Calver, 2001; Freeze & Cherry, 1979). This estimate can be refined by various modifications of rising and falling slug tests and/or grain size analyses. The corresponding potential range of  $t_L$  may help in planning the test duration and test start time, in conjunction with field and weather conditions.

In highly permeable streambeds such as sand and gravel sediments, the time lag  $t_L$  is short, so that visual inspection of the ASM response may be adequate to identify the curvilinear part of the time series data that is needed for accurate joint estimation of parameters  $K_z$  and  $q_z$  by curve fitting. In this case, Equation 24 (or models of varying stream stage from Section 3.3) are applied for standard data interpretation. Tests can be repeated to record stream stage and evaluate  $q_z$  changes over time. The noise amplitude  $A$  can be assessed using statistics of deviations between the field time series and the fitted curve.

In lower conductivity streambeds (e.g., silty sands),  $t_L$  may be on the order of hours or longer, thus the stream stage may vary over this time that will be discussed below. If visual analysis of available time series indicates a lack of curvature in the ASM response, only  $q_z$  can be derived, i.e., using Equations 25 or 26, followed by estimation of  $A$ . Finally, the significance of evaporation and precipitation ( $E$ ) should be assessed for a given test as suggested in Section 3.1, because the interface fluxes  $q_z$  are sometimes of the same order of magnitude as  $E$ , which is commonly on the order of a few mm/day. In many cases,  $E$  can be neglected.

## 4.2. Noise Analysis

A previous study (Solder et al., 2016, Supplemental Information, Appendix C) assessed the standard deviation of error in the inference of  $q_z$  as a function of noise amplitude, while (Solomon et al., 2020, Figure 3) subsequently analyzed the standard deviation in  $K_z$  as a function of test duration  $t_{\text{end}}$ . However, it turns out that errors in  $q_z$  and  $K_z$  depend on noise characteristics as well as on test duration. In practical terms, this means that increasing the test duration may sometimes permit the treatment of noisier data. Therefore, in this study, we analyze relative errors in parameter estimates of  $q_z$  and  $K_z$  as functions of test duration as well as noise amplitude.

### 4.2.1. Synthetic Data

Operating the ASM at one location may include programming of several tests in a sequence by repeatedly opening the valve over long intervals and closing the valve for each individual test (Solomon et al., 2020). Each test over a finite interval  $0 \leq t \leq t_{\text{end}}$  with a closed valve collects  $M$  data points at uniform intervals  $\Delta t = t_{\text{end}}/M$  at times  $t_i = i\Delta t = i \cdot t_{\text{end}}/M$ ,  $i = 0, 1, \dots, M$ . During the period between tests when the valve is opened, measurements of the stream stage  $H_S(t)$  are recorded to verify stream stage stability, possible trends, and identify noise, which is an important part of the data collection process.

To illustrate the synthetic data approach, we consider the case of steady stream stage, i.e.,  $H_S(t) = H_0 = 0$ . In this case, the measurement time series of the water level  $H(t)$  follows the two-parameter Equation 24, namely,  $H(t) = H_{\text{max}}(1 - e^{-t/t_L})$ . Assuming that the values of  $q_z$  and  $K_z$  are known, then the parameters  $H_{\text{max}}$  and  $t_L$  can be calculated directly using Equations 24 and 21.

To analyze the ambient flow and instrumentation errors in a broad range of possible field conditions, we produce a synthetic time series that resembles typically observed field data for an ASM test, which we denote as  $H_F(t_i)$  for  $i = 0, 1, \dots, M$ . For this purpose, a white noise time series  $A \cdot \varepsilon_i$  is added to the value of the theoretical curve at each sample time  $t_i$  (e.g., Solder et al., 2016; Solomon et al., 2020)

$$H_F(t_i) = H_{\text{max}} [1 - \exp(-t_i/t_L)] + A \cdot \varepsilon_i, 0 \leq i \leq M \quad (35)$$

where  $\varepsilon_i \sim N(0,1)$  are independent, identically distributed random variables drawn from the Gaussian distribution with a mean of zero and standard deviation of one, which is consistent with the model. Fitting Equation 24 to the synthetic time series above results in fitted parameters  $H_{\text{max}}^*$  and  $t_L^*$ . We denote the fitted curve by  $H^*(t_i)$ , i.e.

$$H^*(t_i) = H_{\text{max}}^* \left[ 1 - \exp\left(-\frac{i}{M} \frac{t_{\text{end}}}{t_L^*}\right) \right], 0 \leq i \leq M \quad (36)$$

The fitted parameters  $H_{\text{max}}^*$  and  $t_L^*$  can be used to obtain the corresponding values of hydraulic flux and conductivity, which we denote  $q_z^*$  and  $K_z^*$ , using the equations in Section 3. This enables estimation of the relative errors in the parameters  $q_z^*$ ,  $K_z^*$ , and  $H_{\text{max}}^*$ , which we denote by  $\varepsilon_q$ ,  $\varepsilon_K$ , and  $\varepsilon_{H_{\text{max}}}$ . The range of noise amplitude used in generating synthetic data must be a small fraction of the entire range  $H_{\text{max}}$  of water level changes in the upper chamber. If the above model of Gaussian noise is applicable, then at the limit 99.7% of the noisy values synthesized about the curve  $H(t)$  lie within  $H(t) \pm 3A$ , i.e., within a band of range  $6A$ . If the synthetic data is generated from a distribution with greater standard deviation, the synthetic data points may be scattered over the entire range  $H_{\text{max}}$ . Therefore, a practical rule for acceptable synthesized noise amplitude is  $A < H_{\text{max}}/6$ . This noise amplitude model then accounts for both ambient and instrumental noise.

Analysis of Equations 35 and 36 shows that for any values of  $q_z$  and  $K_z$  in a given location, the estimates can be presented using the two dimensionless parameters  $A/H_{\text{max}}$  and  $t_{\text{end}}/t_L$  for any specified number of measurements  $M$ .

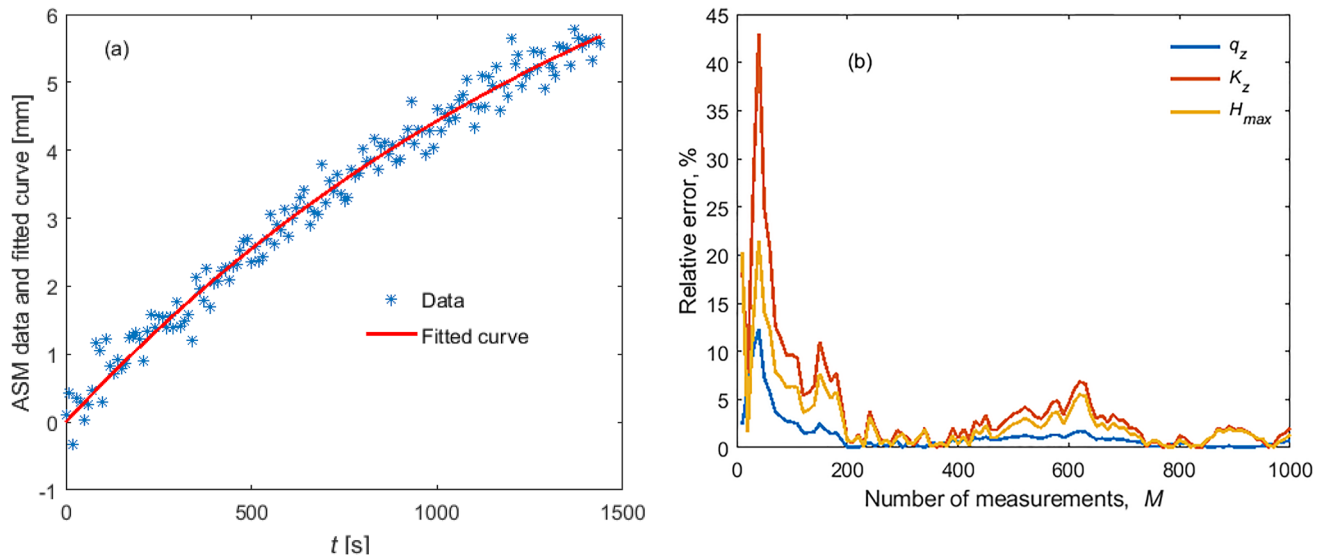


**Figure 2.** Response curve analysis of the Automatic Seepage Meter test: (a) synthetic data and the best fit; (b) effect of the number of data points  $M$  on relative error of parameter identification.

#### 4.2.2. Methodology for Interpreting Synthetic Field Data

The fitting of Equation 24 to the synthetic field data generated using Equation 35 can be accomplished using a least squares approach, and specifically by searching for the minimum value of the objective function  $\sum_{i=1}^M [H_F(t_i) - H^*(t_i)]^2$ . For this purpose, we employ the Nelder-Mead simplex algorithm (Lagarias et al., 1998), which is implemented as the routine `fminsearch` for multidimensional unconstrained nonlinear minimization in MATLAB. The basic script for the computation described below can be found in Text S2 in Supporting Information S1.

An example of synthetic noise in the ASM data generated by MATLAB command `randn` is shown in Figure 2a for a streambed with nominal parameters  $K_z = 14.4 \text{ m day}^{-1}$  and  $q_z = 0.5 \text{ m day}^{-1}$  (details are given in Text S2 in Supporting Information S1). For an ASM with  $L = 0.30 \text{ m}$ , these parameters lead to a time-lag value of  $t_L = 1,800 \text{ s}$  according to Equation 21, where  $F = 1$  is assumed, and then the maximal rise is  $H_{\max} = 10.4 \text{ mm}$ . A test duration at 80% of  $t_L$  is chosen, resulting in  $t_{\text{end}} = 1,440 \text{ s}$ . The time step  $\Delta t = 10 \text{ s}$  results in a total number of  $M = 144$  collected data points. The standard deviation for the synthetic noise distribution  $H_{\max}$  is chosen as  $A = 0.2 \text{ mm}$ . Note that 99.7% of samples generated from a normal distribution  $N(0, A)$  with mean 0 and standard deviation  $A$  are within the bandwidth  $\pm 3A$ , i.e., within a range of  $6A = 1.2 \text{ mm}$ , or about 12% of the terminal water level rise  $H_{\max}$ . Application of the curve fitting algorithm using a relative error tolerance  $\epsilon_{\text{tol}} = 10^{-4}$  for terminating the optimization results in estimates of the parameters  $q_z$ ,  $K_z$ , and  $H_{\max}$  with relative errors of 2.2%, 9.3%, and 6.5%, respectively (Figure 2a).

In practice, uniform time intervals  $t_{i+1} - t_i = \Delta t$  between measurements are used throughout the test duration from initiation until  $t_{\text{end}}$ , and the estimation accuracy can vary significantly with the number of measurements  $M$ . Instead of  $M = 144$ , we examined various sampling sizes  $M$  of uniformly distributed measurements ranging between 10 and 1,000. Figure 2b shows that the relative errors in parameter estimation do not change uniformly. We do, however, observe that the error  $\epsilon_q$  in  $q_z$  is generally  $< 3\%$  when  $M > 100$  data points, and the error  $\epsilon_K$  in  $K_z$  is  $< 3\%$  for sampling sizes of  $200 < M < 400$ . In the numerical experiment shown in Figure 2b, the array of noise samples that was used to create the synthetic time series array was extended by adding generated random numbers for each increment in  $M$ , retaining the samples generated for the previous value of  $M$ .

To illustrate the accuracy of the parameter inference from noisy data, the test results from Figure 2a were revisited in order to examine how changing  $t_{\text{end}}$  and  $A$  affects relative errors in the estimates of  $q_z$ ,  $K_z$ , and  $H_{\max}$ . Figure 3a compares the relative error in estimates of the parameters  $q_z$ ,  $K_z$ , and  $H_{\max}$  as  $t_{\text{end}}$  increases while the standard deviation of the synthetic measurement noise is fixed at  $A = 0.2 \text{ mm}$ . For each numerical experiment, there were

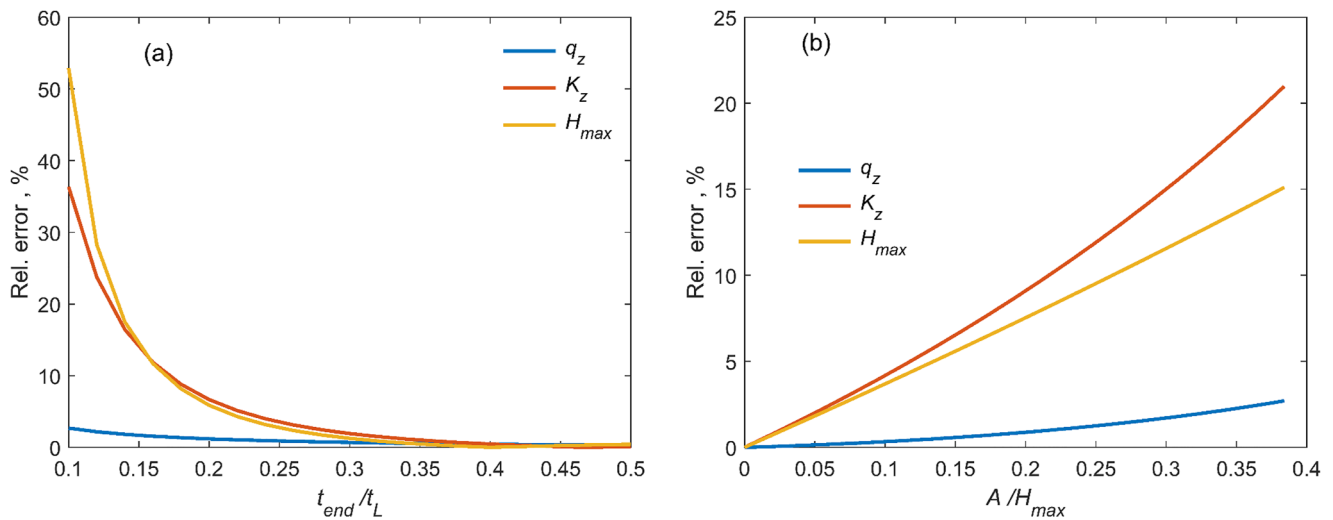


**Figure 3.** Examples of relative errors of joint estimation of  $q_z$  and  $K_z$  as functions of (a) duration  $t_{end}$  of the test, and (b) noise amplitude ( $A$ ).

$M = 200$  measurement points uniformly distributed over the test interval  $t_{end}$ . Alternatively,  $\Delta t$  could be fixed for the different tests, but this would change the number of data points  $M$  for each test duration  $t_{end}$ .

The results in Figure 3 clearly indicate a reduction of estimation error as the ratio of the test duration to the time lag  $t_{end}/t_L$  in general. However, the parameters  $q_z$  and  $K_z$  are determined with different accuracy, which is apparent from comparing Equations 25 and 26. The value of  $q_z$  is largely defined by the slope of the initial segment on the water level curve but finding  $K_z$  requires a segment of the curve that exhibits curvature, which develops at  $t \approx 0.4 \cdot t_L$  and later. One can achieve higher accuracy for both  $q_z$  and  $K_z$  by extending  $t_{end}$ .

To estimate parameters from noisy data with acceptable accuracy, it is important that the range of data points ( $\approx 6A$ ) should be less than  $H_{max}$ , i.e.,  $A/H_{max} < 1/6$ , as explained above. Figure 3b illustrates the effect of the noise on relative errors for fixed test duration  $t_{end} = 1,440$  s. The key conclusion from this example is that noise increases errors in the estimate of  $q_z$ , but these errors remain within practically acceptable bounds. Meanwhile, errors in the estimate of  $K_z$  increase substantially with  $A$ , but (Bouwer, 1996) acknowledged that errors on the order of 25% are acceptable for practical applications. The error in measurements of the stream stage  $H_s(t)$  may vary at a given location, together with  $A/H_{max}$ , and the result in Figures 2 and 3 indicate that parameter estimation error may be reduced by selecting appropriate test timing.

#### 4.2.3. Effect of Test Duration, Noise Level, and Number of Measurements on Joint Parameter Estimation Accuracy

The accuracy of estimating  $q_z$  and  $K_z$  jointly by fitting to data obtained from a single test can be examined with respect to the dimensionless parameters  $t_{end}/t_L$  and  $A/H_{max}$ , as examined in Figure 3 in the previous section. We analyze the influence of these parameters using the same nominal aquifer parameter values used in Section 4.2.2. In addition, we compare the results of the estimation method using the recommended number of collected measurements  $M = 150$  with a reduced number ( $M = 50$ ). The results are shown in Figure 4.

The ratio  $t_{end}/t_L$  is in the range from 0.2 to 1.0 for most anticipated ASM and streambed characteristics and field situations. The accuracy of an ASM test with shorter duration for estimation of  $K_z$  significantly decreases because of the effects of noise, which obscures the early onset of the curvilinear section. The parameter  $A/H_{max}$  can vary in the range from 0 for noiseless data to about 1/6, so we choose  $A/H_{max}$  ranging from 0 to 0.08 for illustration.

Each numerical experiment uses  $M = 150$  measurements, which is consistent with the recommendations above. It is apparent that at any noise amplitude, the error  $\epsilon_q$  (i.e., 5%–10%) is lower than  $\epsilon_K$  (about 20%) for a similar noise level. The noise amplitude parameter  $A/H_{max} < 0.04$  shown on the diagram for  $\epsilon_q$  is satisfactory if an estimation error of 5% is satisfactory. However, when  $0 < t_{end}/t_L < 0.4$ , the influence of noise degrades the accuracy of the result. For example, an early termination of the test at  $t_{end}/t_L = 0.3$  reduces estimation accuracy to 10%. Further shortening of the test gives progressively higher errors unless the noise level is also smaller. For example,



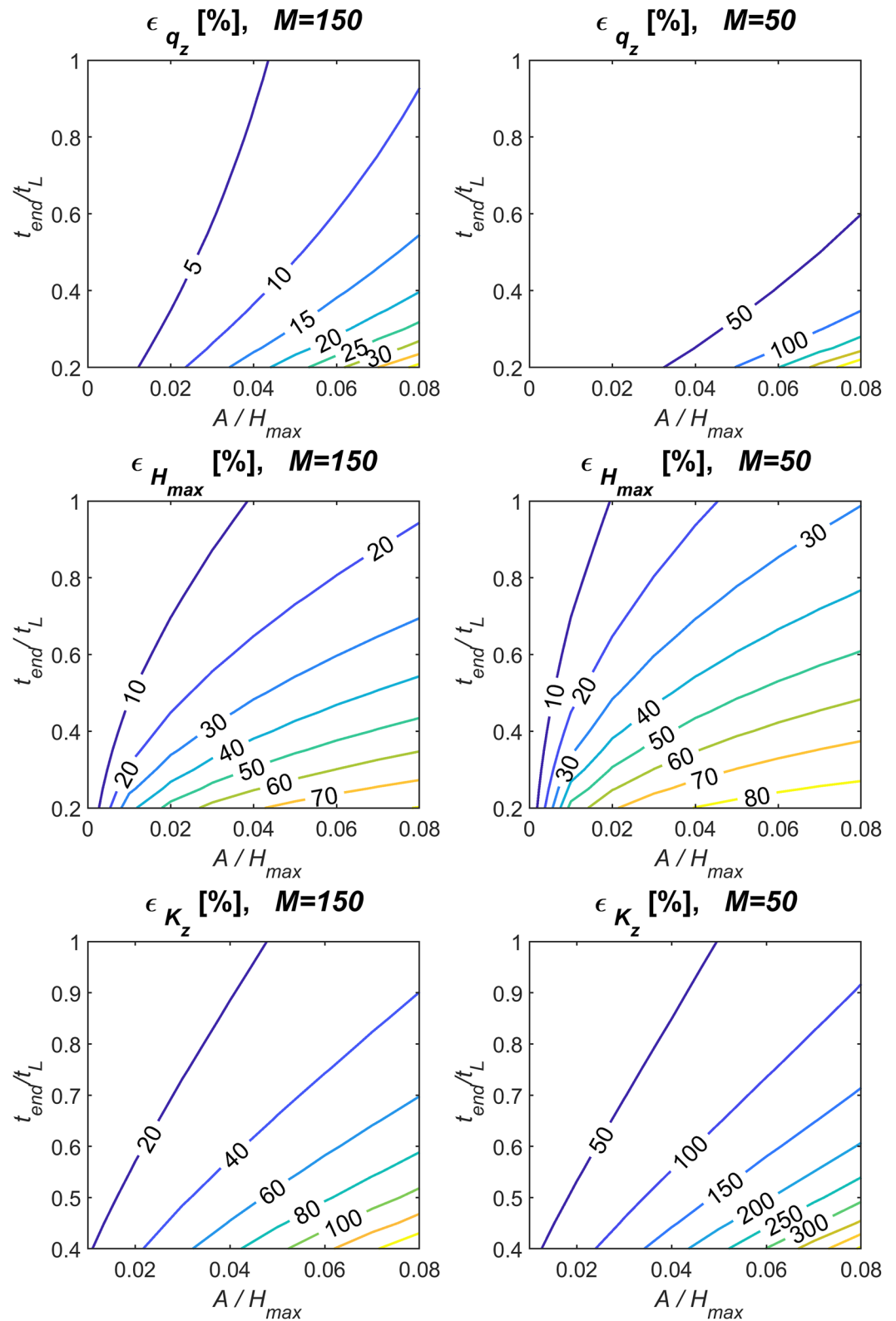


**Figure 4.** Analysis of errors in the Automatic Seepage Meter test. Empirical error  $\epsilon_q$ ,  $\epsilon_{K_z}$ , and  $\epsilon_{H_{max}}$  (in %) in estimates of  $q_z$ ,  $H_{max}$ , and  $K_z$ , and given in the top, middle, and bottom rows, respectively. Effect of the number of measurements on accuracy is shown by comparison between left and right columns, with  $M = 150$  and  $M = 50$  measurements, respectively.



an accuracy of 5% can be achieved for noise amplitude that satisfies  $A/H_{\max} < 0.035$ . The general rule is that an increase of test duration, or  $t_{\text{end}}/t_L$  is expected to increase the accuracy of results for any specific noise level, but this improvement depends on the noise amplitude.

This analysis can be used for understanding errors in parameter estimates using ASM test results, and to calibrate  $t_{\text{end}}/t_L$  and  $A/H_{\max}$  to improve the accuracy of anticipated inference. For this purpose, the noise amplitude  $A$  can be inferred based on parameter estimates instead of known values. In that case, diagrams like Figure 4 can be constructed using numerical experiments like those described above, which can then be used to determine the most suitable values of  $t_{\text{end}}/t_L$  and  $A/H_{\max}$  that are expected to yield the most accurate parameter estimates. Recognition of the error in estimates of  $q_z$  motivated the switch from a pressure transducer measurement of  $H$  (Solder et al., 2016) to an electromechanical method (Solomon et al., 2020), which can achieve noise amplitudes as low as  $A < 10^{-4}$  m.

Moreover, such analysis has ramifications for the selection of the instrument characteristics. Because commonly observed values of  $H_{\max}$  are on the order of 0.001–0.1 m, a parameter value of  $A/H_{\max} < 0.1$  requires noise amplitude  $A$  to be in the range of  $10^{-4}$ – $10^{-2}$  m. At the upper bound of the range, the accuracy of standard pressure transducers is quite adequate. The lower bound is in micron range, and the sensitivity of traditional pressure transducers becomes inadequate, while the ASM (Solomon et al., 2020) produces data from which parameters can be estimated with acceptable accuracy. The last remark is related to the length of the measurement time series. Plots for  $M = 50$  in Figure 4 clearly illustrate the deterioration of accuracy of data interpretation compared to  $M = 50$ .

### 4.3. Accelerating the ASM Test by Changing Geometry

As shown in Section 4.2, the accuracy of ASM tests increases with an increase of the ratio  $t_{\text{end}}/t_L$ , i.e., a reduction of  $t_L$  or an increase of  $t_{\text{end}}$ . The time lag  $t_L$  can be controlled by the ASM geometry streambed parameters  $R$  and  $L$  (Solder et al., 2016; Zlotnik et al., 2021, Figure 1b). Also, outfitting the upper chamber with an amplifier, which is a tube of smaller radius  $R_A < R$  on the top, further leads to the modified time lag  $t_A$ , which takes the form

$$t_A = t_L \left( \frac{R_A}{R} \right)^2 = \frac{LF}{K_z} \left( \frac{R_A}{R} \right)^2 \quad (37)$$

resulting in an adjusted Equation 24 for the water level in the ASM of form

$$H(t) = H_0 + H_{\max} \left( 1 - e^{-\frac{t}{t_A}} \right), H_{\max} = q_z t_L \quad (38)$$

The modified time lag  $t_A$  indicates that the water level approaches its terminal value of  $H_{\max} = q_z t_L$  faster, where  $t_L$  is estimated given parameters  $R$  and  $L$ , but is unchanged by the addition of an amplifier. An alternative is to use a lower chamber with a wider radius and reduced penetration depth. Then the ASM can be used as the amplifier attached to the large diameter lower chamber. Commonly, isotropic conditions are assumed for the scales of an ASM test based on typical data by (Burger & Belitz, 1997). Moreover (Zlotnik et al., 2021, Equation 22 and Table 1), presented  $F$  as a monotonic function of the dimensionless parameter  $R^* = (R/L)\sqrt{K_z/K_r}$ , with empirical coefficient values, and of form

$$F = F_a(R^*) = \exp[0.435710 + 0.326818 * \ln(R^*) + 0.0786683 * (\ln(R^*))^2 + 0.00169158 * (\ln(R^*))^3 - 0.00095506 * (\ln(R^*))^4] \quad (39)$$

A decrease of  $L$  reduces  $t_L$  and  $t_A$ , but simultaneously reduces  $H_{\max}$ . Therefore, one must evaluate the tradeoffs between accuracy and time  $t_{\text{end}}$  in the test designs. Here, we only indicate the possibilities of accelerating  $t_{\text{end}}$  by orders of magnitude.

## 5. Applications

We demonstrate the ASM data analysis method developed in this study using examples from two sites: Hominy Swamp Creek in Wilson, North Carolina (Nickels et al., 2023) and the South Branch of the Middle Loup River, Nebraska (Gilmore et al., 2020). The data and their descriptions, including test locations and dates, can be found in the CUASHI HydroShare repository (Zlotnik et al., 2023).

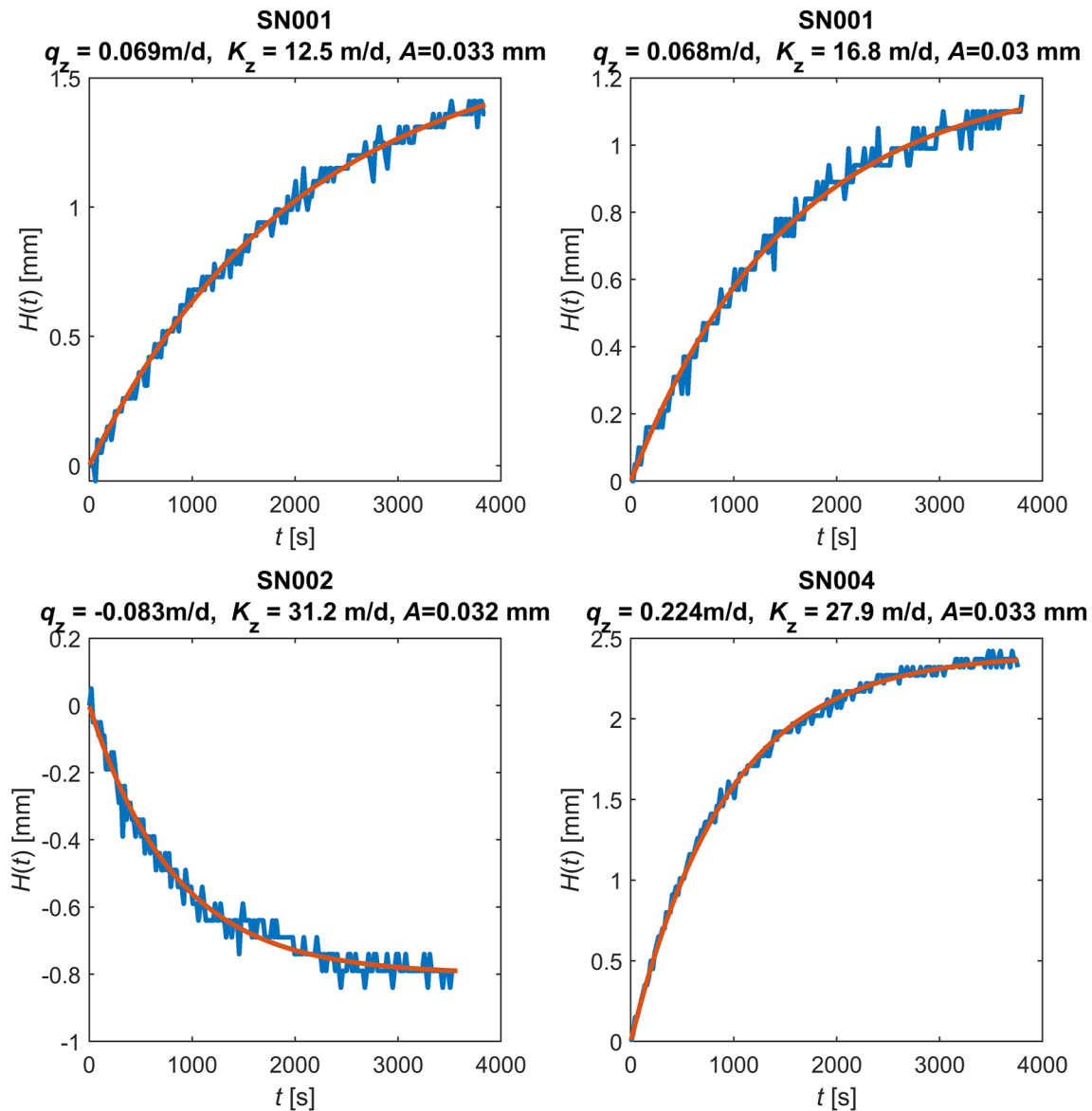


**Figure 5.** Automatic Seepage Meter responses at different locations in the streambed at Hominy Swamp Creek, North Carolina: field data in blue and fitted curves in red.

### 5.1. Hominy Swamp Creek, North Carolina

The ASM test results at Hominy Swamp Creek were collected in October 2015 with time intervals of 19 s. Visual analysis (Figure 5) indicates presence of curvilinear sections in the ASM responses. The hydraulic conductivity  $K_z$  is consistent with data for alluvial streambed sediments (Calver, 2001). The streambed has a mean vertical hydraulic conductivity of  $18.4 \text{ m day}^{-1}$  with a minimum of  $0.025 \text{ m day}^{-1}$  and a maximum of  $70.5 \text{ m day}^{-1}$  (Nickels et al., 2023).

The results in Figure 5 show a relatively high range of hydraulic conductivity corresponding to the medium to coarse sand and noise amplitude at  $A \approx 0.03 \text{ mm}$ . The two upper plots present test data collected at location SN001 using the same tube without removal. The interval between two tests was 4 hr, indicating consistent upward groundwater flux. It is important to note the small difference between values of  $q_z$ , at just about 1%, while the amplitude varies by about 5%–10%. However, the test data at location SN002 indicate a losing stream location (downward ambient water flux through the streambed), and test data SN004 indicate another gaining location.

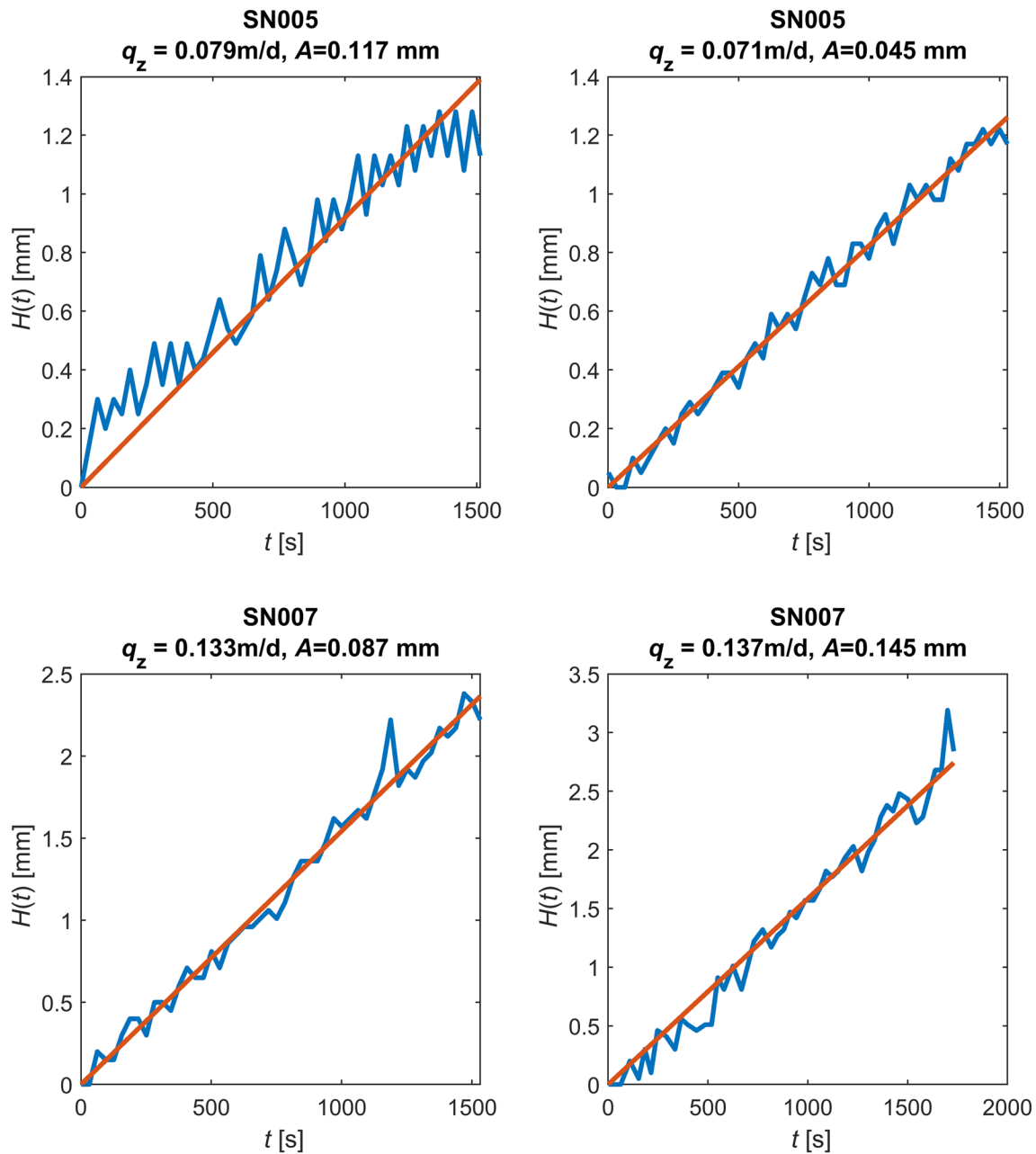


Figure 6. Automatic Seepage Meter responses at different locations at the South Branch of the Middle Loup River, Nebraska site: data in blue and fitted curves in red.

### 5.2. South Branch of the Middle Loup River, Sand Hills, Nebraska

The ASM test data from the South Branch of the Middle Loup River (Figure 6) were collected in summer 2018 (Solomon et al., 2020), with a time interval of 31 s. Visual analysis of the roughly 25-min-long data series show a linear ASM response, and the lack of a curvilinear part precludes estimation of  $K_z$ .

### 5.3. Best Practice for Determining ASM Test Measurement Protocols

We complete our study with a numerical analysis to determine the optimal ASM data collection protocols for minimizing the errors  $\epsilon_q$ ,  $\epsilon_{K_z}$ , and  $\epsilon_{H_{\max}}$  in the joint estimates of  $q_z$ ,  $K_z$ , and  $H_{\max}$ . First, we observe that based on the experiments shown in Figure 2b, a time series of  $M = 200$  measurements results in low estimation error, and the analysis in Figure 4 confirms that the errors will decrease for a broad range of values of  $t_{\text{end}}/t_L$  and  $A/H_{\max}$ . We then

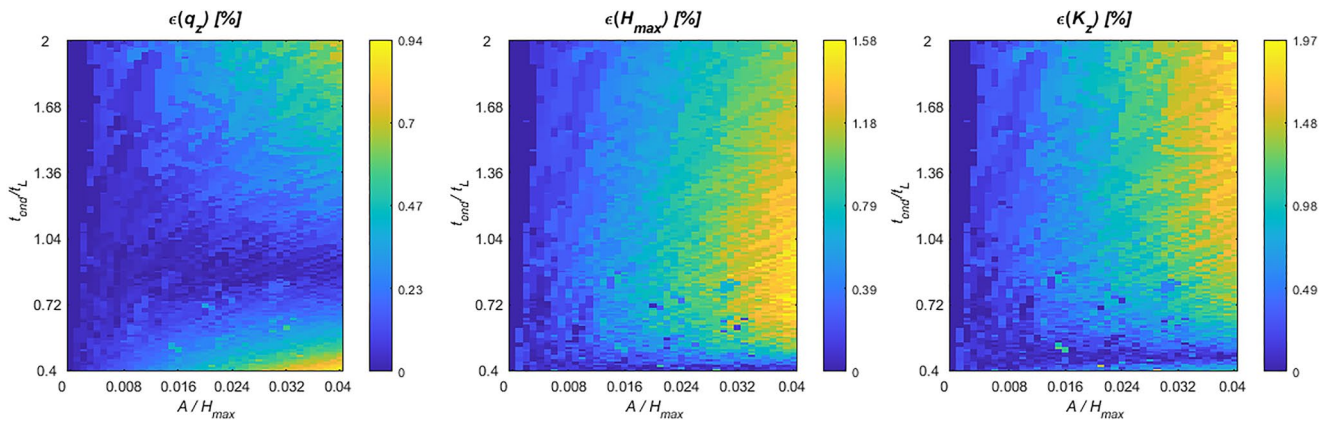


**Figure 7.** Simulation of errors in an Automatic Seepage Meter test using synthetic data generated using SN001 parameters  $q_z = 0.069 \text{ m day}^{-1}$ ,  $K_z = 12.5 \text{ m day}^{-1}$ , and  $A = 0.033 \text{ mm}$  with  $M = 200$  synthetic measurements. Empirical errors  $\epsilon_{q_z}$ ,  $\epsilon_{H_{\max}}$ , and  $\epsilon_{K_z}$  (in %) in estimates of  $q_z$ ,  $H_{\max}$ , and  $K_z$  are shown at left, center, and right, respectively.

perform a collection of parameter estimation experiments using synthetic data as described in Section 4.2. The synthetic data in each instance are generated for the parameters  $q_z = 0.069 \text{ m day}^{-1}$ ,  $K_z = 12.5 \text{ m day}^{-1}$ , and  $A = 0.033 \text{ mm}$  estimated using the ASM test response data SN001 obtained at the Hominy Swamp Creek site, with data and curve fit shown at top left in Figure 5. Synthetic measurement data with  $M = 200$  are generated, and the empirical errors in curve fits are shown in Figure 7.

Because we have chosen  $M = 200$ , we find that the estimation errors  $\epsilon_{q_z}$ ,  $\epsilon_{H_{\max}}$ , and  $\epsilon_{K_z}$  are all quite low,  $<2\%$ , for all examined values of  $t_{\text{end}}/t_L$  and  $A/H_{\max}$ . Clearly, lower noise amplitude results in lower estimation error in nearly all cases. However, we see that different test durations  $t_{\text{end}}/t_L$  result in different estimator performance. In particular, values of  $t_{\text{end}}/t_L \approx 0.4$  result in very low error for estimating  $K_z$  and  $H_{\max}$ , with values of  $<0.5\%$ , and values of  $t_{\text{end}}/t_L \approx 1$  result in very low error for estimating  $q_z$ , with  $\epsilon_{q_z} < 0.25\%$ . In the latter case, the hydraulic flux  $q_z$  can be estimated with relative error  $\epsilon_{q_z} < 0.25\%$  for any of the examined noise amplitudes, even up to  $A/H_{\max} = 0.04$ .

## 6. Conclusions

1. This study presents a theory to characterize the measurements obtained by the ASM test based on a rigorous 3D hydrodynamic analysis. The dynamics of the time-varying water level inside the ASM tube can be reduced to an ordinary linear differential equation. This general solution accounts for a wide range of ASM tests by including the shape factor with streambed anisotropy in hydraulic conductivity, transient stream stage, and varying fluxes across the interface, as well as evaporation and precipitation during the test, and most importantly, measurement noise.
2. In case of steady-state stream stage, the solution is shown to reduce to the basic equation of Solomon et al. (2020, Equation 1), but the shape factor  $F$  is corrected for given tube radii and penetration as outlined by Zlotnik et al. (2021). The systematic error is on the order of 9% for the existing configuration of the ASM, and changes in radius or penetration depth can change this error.
3. The general solution for the ASM test responses also accounts for linear and piecewise-linear stream stage variations. It was rigorously proven that the solution for piecewise-constant stream stage converges to Solomon et al. (2020, Equation 7) in a special case.
4. Linear stream stage dynamics may result in nonmonotonic changes of the flow direction in the ASM water level when their directions do not coincide, as was empirically found by Solomon et al. (2020). Here, the criterion for the existence and timing of this phenomenon ( $t_{\text{ch}}$ ) was derived as a function of time lag  $t_L$ , water flux  $q_z$ , and the rate of stream stage changes in Equation 29.
5. The method of simultaneously determining vertical water flux and vertical hydraulic conductivity of streambed sediments from the same data set in one algorithm is analyzed in detail. Analyses show that this approach is accurate (on the order of a few percent) when ASM water level data exhibit a curvilinear segment and low noise (e.g., Figure 5).
6. The physical meaning of a hypothesized parabolic approximation of the water level dynamics (see Solomon et al., 2020) was obtained from first principles, with process-based explanation of the coefficients

(Equation 25). In particular, a quadratic term allows for inferring vertical hydraulic conductivity from the same data (in addition to  $q_z$ ), and analysis of the accuracy of this approximation is presented in terms of the test duration  $t_{\text{end}}/t_L$ .

7. We propose the use of numerical simulations using synthetic data to generate diagrams for finding the proper combination of test duration and noise level to estimate  $q_z$  and  $K_z$  with required accuracy (Figure 4). Using this approach, the anticipated accuracy in the estimates of  $q_z$  and  $K_z$  can be calibrated by the choice of test duration  $t_{\text{end}}$  (defined by the ratio  $t_{\text{end}}/t_L$ ) and the noise amplitude  $A$  (defined by the ratio  $A/H_{\text{max}}$ ).
8. The tradeoff between test duration and noise level is important for accurate interpretation of the data. Any noise  $A/H_{\text{max}} < 0.1$  is acceptable, if  $t_{\text{end}}/t_L > 0.4$  and error up to 5% is satisfactory. However, earlier truncation of the test may reduce accuracy significantly, and the noise amplitude will determine the accuracy of the result. Shortening the test gives progressively higher errors unless it is accompanied by a corresponding reduction of ambient noise and/or increasing accuracy of water level measurements.
9. This theory can be useful for ASM design improvements for test time optimization. Modifications of the ratio of tube radius to tube penetration depth ( $R/L$ ) and the addition of an amplifier with radius  $R_A < R$  may result in reduction of the time lag  $t_L$ , which would enable more tests, both spatially and temporally.

## Notation

$E$	difference between evaporation and precipitation rates
$F$	shape factor
$h(r, z, t)$	local head in cylindrical coordinates ( $r, z$ )
$h_0(r, z, t)$	local head in undisturbed conditions
$H(t), H^*(t_i)$	water level in the ASM as a continuous function of time and its measurement
$H_{\text{max}}$	maximum level change in the ASM
$H_S(t)$	stream stage
$i$	number of a point in time series from the ASM
$I$	maximum number of intervals in interpolated time series from the ASM
$K_r, K_z$	horizontal and vertical hydraulic conductivity
$L$	penetration depth
$M$	number of points in time series from the ASM
$N(0, 1)$	normal distribution with mean equal to zero and standard deviation of one
$p, p_i$	slope of linear stream stage record and slope of $i$ th segment of the stream stage record
$q_z, q_z^*$	vertical flux across the interface and estimate (includes errors)
$Q(t)$	discharge across interface between chambers due to head difference and natural gradient
$Q_{\text{OBP}}(t)$	discharge across the interface between chambers without natural gradient
$R$	tube radius
$s(r, z, t)$	drawup
$S_s$	specific storage
$t, t_i$	continuous time and time of $i$ th measurement
$t_L, t_L^*$	time lag, actual and evaluated from field data
$t_{\text{end}}$	test duration
$\epsilon_{q_z}, \epsilon_{K_z}, \epsilon_{H_{\text{max}}}$	relative errors of parameter estimates

## Data Availability Statement

The measured ASM water level changes at two field sites, used in this paper can be retrieved from CUASHI web site <https://www.cuahsi.org/>. Data can be downloaded (Zlotnik et al., 2023) from HydroShare: <https://doi.org/10.4211/hs.18ffc61b69fe49debd99edc407cbcbaa>.

## Acknowledgments

The authors gratefully acknowledge financial support of this work from the U.S. National Science Foundation through awards 1744714 (NC State University), 1744719 (University of Nebraska), and 1744721 (University of Utah).

## References

- Bardini, L., Boano, F., Cardenas, M. B., Sawyer, A. H., Revelli, R., & Ridolfi, L. (2013). Small-scale heterogeneity has negligible effects on nutrient cycling in streambeds. *Geophysical Research Letters*, *40*, 1118–1122. <https://doi.org/10.1002/grl.50224>
- Boano, J., Harvey, W., Marion, A., Packman, A. I., Revelli, R., Ridolfi, L., & Wörman, A. (2014). Hyporheic flow and transport processes: Mechanisms, models, and biogeochemical implications. *Reviews of Geophysics*, *52*, 603–679. <https://doi.org/10.1002/2012RG000417>



- Bouwer, H. (1978). *Groundwater hydrology*. McGraw-Hill. ISBN: 0070067155 9780070067158.
- Bouwer, H. (1996). Discussion of Bouwer and Rice slug test review articles. *Groundwater*, 34(1), 1–171.
- Burger, R. L., & Belitz, K. (1997). Measurement of anisotropic hydraulic conductivity in unconsolidated sands: A case study from a shoreface deposit, Oyster, Virginia. *Water Resources Research*, 33(6), 1515–1522. <https://doi.org/10.1029/97WR00570>
- Burnette, M., Genereux, D. P., & Birgand, F. (2016). *In-situ* falling-head test for hydraulic conductivity: Evaluation in layered sediments of an analysis derived for homogenous sediments. *Journal of Hydrology*, 539, 319–329. <https://doi.org/10.1016/j.jhydrol.2016.05.030>
- Calver, A. (2001). Riverbed permeabilities: Information from pooled data. *Groundwater*, 39(4), 546–553. <https://doi.org/10.1111/j.1745-6584.2001.tb02343.x>
- Chen, X., Song, J., Cheng, C., Wang, D., Lackey, S. O., & Song, J. (2009). A new method for mapping variability in vertical seepage flux in streambeds. *Hydrogeology Journal*, 17(10), 519–525. <https://doi.org/10.1007/s10040-008-0384-0>
- Chen, X. H. (2000). Measurement of streambed hydraulic conductivity and its anisotropy. *Environmental Geology*, 39(12), 1317–1324. <https://doi.org/10.1007/s002540000172>
- Creameans, M., Devlin, J., Osorno, T., McKnight, U., & Bjerg, P. (2020). A comparison of tools and methods for estimating groundwater-surface water exchange. *Ground Water Monitoring Review*, 40(1), 24–34. <https://doi.org/10.1111/gwmr.12362>
- Freeze, A., & Cherry, J. (1979). *Groundwater*. Prentice Hall. ISBN: 0-13-365312-9.
- Gilmore, T. E., Genereux, D. P., Solomon, D. K., & Solder, J. E. (2016). Groundwater transit time distribution and mean from streambed sampling in an agricultural coastal plain watershed, North Carolina, USA. *Water Resources Research*, 52, 2025–2044. <https://doi.org/10.1002/2015WR017600>
- Gilmore, T. E., Johnson, M., Korus, J., Mittelstet, A., Briggs, M. A., Zlotnik, V., & Corcoran, S. (2020). Streambed flux measurement informed by distributed temperature sensing leads to a significantly different characterization of groundwater discharge. *Water*, 11, 2312. <https://doi.org/10.3390/w11112312>
- Glose, T. J., Lowry, C. S., & Hausner, M. B. (2019). Limits on groundwater-surface water fluxes derived from temperature time series: Defining resolution-based thresholds. *Water Resources Research*, 55, 10678–10689. <https://doi.org/10.1029/2019WR025643>
- Humphrey, C. E., Solomon, D. K., Genereux, D. P., Gilmore, T. E., Mittelstet, A. R., Zlotnik, V. A., et al. (2022). Using automated seepage meters to quantify the spatial variability and net flux of groundwater to a stream. *Water Resources Research*, 58, e2021WR030711. <https://doi.org/10.1029/2021WR030711>
- Hvorslev, M. J. (1951). *Time lag and soil permeability in groundwater observations*. Waterways Experiment Station, Corps of Engineers, U.S. Army. Bulletin No. 36.
- Kennedy, C. D., Genereux, D. P., Corbett, D. R., & Mitasova, H. (2009). Spatial and temporal dynamics of coupled groundwater and nitrogen fluxes through a streambed in an agricultural watershed. *Water Resources Research*, 45, W09401. <https://doi.org/10.1029/2008WR007397>
- Kennedy, C. D., Murdoch, L. C., Genereux, D. P., Corbett, D. R., Stone, K., Pham, P., & Mitasova, H. (2010). Comparison of Darcian flux calculations and seepage meter measurements in a sandy streambed in North Carolina, USA. *Water Resources Research*, 46, W09501. <https://doi.org/10.1029/2009WR008342>
- Lagarias, J. C., Reeds, J. A., Wright, M. H., & Wright, P. E. (1998). Convergence properties of the Nelder-Mead simplex method in low dimensions. *SIAM Journal on Optimization*, 9(1), 112–147. <https://doi.org/10.1137/S1052623496303470>
- Landon, M. K., Rus, D. L., & Harvey, F. E. (2001). Comparison of instream methods for measuring hydraulic conductivity in sandy streambeds. *Groundwater*, 39(6), 870–885. <https://doi.org/10.1111/j.1745-6584.2001.tb02475.x>
- Liu, Y., Jiao, J. J., & Cheng, H. K. (2018). Tracing submarine groundwater discharge flux in Tolo Harbor, Hong Kong (China). *Hydrogeology Journal*, 26, 1857–1873. <https://doi.org/10.1007/s10040-018-1736-z>
- Nickels, J. L., Genereux, D. P., & Knappe, D. R. U. (2023). Improved Darcian streambed measurements to quantify flux and mass discharge of volatile organic compounds from a contaminated aquifer to an urban stream. *Journal of Contaminant Hydrology*, 253, 104124. <https://doi.org/10.1016/j.jconhyd.2022.104124>
- Pétrié, M.-A., Genereux, D. P., Koropecjy-Cox, L., Knappe, D. R. U., Dubosq, S., Gilmore, T. E., & Hopkins, Z. (2021). Per- and polyfluoroalkyl substance (PFAS) transport from groundwater to streams near a PFAS manufacturing facility in North Carolina, USA. *Environmental Science & Technology*, 55(9), 5848–5856. <https://doi.org/10.1021/acs.est.0c07978>
- Pozdnyakov, S. P., Wang, & P., & Lekhov, M. (2016). A semi-analytical generalized Hvorslev formula for estimating riverbed hydraulic conductivity with an open-ended standpipe permeameter. *Journal of Hydrology*, 540, 736–743. <https://doi.org/10.1016/j.jhydrol.2016.06.061>
- Rosenberry, D. O., & Hayashi, M. (2013). Assessing and measuring wetland hydrology. In J. S. Anderson, & D. A. Davis (Eds.), *Wetland techniques—Volume 1: Foundations* (pp. 87–225). Springer. ISBN: 978-94-007-6859-8. [https://doi.org/10.1007/978-94-007-6860-4\\_3](https://doi.org/10.1007/978-94-007-6860-4_3)
- Rosenberry, D. O., LaBaugh, J. W., & Hunt, R. J. (2008). Use of monitoring wells, portable piezometers, and seepage meters to quantify flow between surface water and ground water. In D. O. Rosenberry, & J. W. LaBaugh (Eds.), *Field techniques for estimating water fluxes between surface water and ground water*. Techniques and Methods Chapter 4-D2. U.S. Department of the Interior, U.S. Geological Survey. (Chap. 2). Retrieved from <https://pubs.usgs.gov/tm/04d02/pdf/TM4-D2-chap2.pdf>
- Solder, J., Gilmore, T., Genereux, D., & Solomon, D. K. (2016). A tube seepage meter for in situ measurement of seepage rate and groundwater sampling. *Groundwater*, 54(4), 588–595. <https://doi.org/10.1111/gwat.12388>
- Solomon, D. K., Humphrey, E., Gilmore, T. E., Genereux, D. P., & Zlotnik, V. A. (2020). An automated seepage meter for streams and lakes. *Water Resources Research*, 56, e2019WR026983. <https://doi.org/10.1029/2019WR026983>
- Tartakovsky, D. M., Moulton, J. D., & Zlotnik, V. A. (2000). Kinematic structure of mini-permeameter flow. *Water Resources Research*, 36, 2433–2442. <https://doi.org/10.1029/2000WR900178>
- Zlotnik, V., & Ledder, G. (1996). Theory of dipole flow in uniform anisotropic aquifers. *Water Resources Research*, 32(3), 1119–1128. <https://doi.org/10.1029/95WR03813>
- Zlotnik, V., & Tartakovsky, D. (2018). Interpretation of heat-pulse tracer tests for characterization of three-dimensional velocity fields in hyporheic zone. *Water Resources Research*, 54, 4028–4039. <https://doi.org/10.1029/2017WR022476>
- Zlotnik, V. A., Cole, K. D., Cardenas, M. B., & Zlotnik, A. V. (2021). Enabling the application of large footprint open-bottom permeameters through new shape factors. *Water Resources Research*, 57, e2020WR029315. <https://doi.org/10.1029/2020WR029315>
- Zlotnik, V. A., Solomon, D. K., Gilmore, T. E., Genereux, D., Humphrey, C. E., Mittelstet, A. R., & Zlotnik, A. V. (2023). Theory of Automatic Seepage Meter and ramifications for applications. HydroShare [Dataset]. <https://doi.org/10.4211/hs.18ffc61b69fe49deb99edc407cbcbaa>
- Zlotnik, V. A., Ward, A., Harvey, J., Lautz, L., Rosenberry, D., & Brunner, P. (2016). Ch. 9. Groundwater-surface water interactions. In J. Cushman, & D. Tartakovsky (Eds.), *Handbook of groundwater engineering* (3rd ed., pp. 237–288). Taylor and Francis. <https://doi.org/10.1201/9781315371801>